Agricultural and Forest Meteorology 350 (2024) 110000

Contents lists available at ScienceDirect

Agricultural and Forest Meteorology

journal homepage: www.elsevier.com/locate/agrformet

Surface-layer turbulence associated with a fast spreading grass fire

Shiyuan Zhong [a,*], Melissa Gonzalez-Fuentes [b], Craig B. Clements [b], Xindi Bian [c], Warren E. Heilman [c], Joseph J. Charney [c], Mario M. Valero [b,d], Adam K. Kochanski [b], Michael T. Kiefer [a]

[a] Michigan State University, East Lansing, MI, USA
[b] San José State University, San José, CA, USA
[c] US Forest Service, Northern Research Station, East Lansing, MI, USA
[d] Universitat Politècnica de Catalunya, Barcelona, Spain

A R T I C L E I N F O

Keywords:
Turbulence
Wildland fire
Fire-Atmosphere Interaction
Fire behavior
Flux tower
Sonic anemometer

A B S T R A C T

A wildland fire experiment was conducted on a 40-ha tall grass prairie in Texas to study fire-atmosphere interactions. The experiment coincided with a Red Flag Warning, signifying specific weather conditions associated with an elevated risk of wildfire ignition and rapid spread. This provided a rare opportunity to observe wildland fire behavior and its impact on atmospheric flows under conditions deliberately avoided in similar experiments. This study analyzed the high frequency meteorological data collected during the experiment using three-dimensional sonic anemometers mounted on a 43-m tower (at 5.8, 10 and 20 m) and on three 10-m towers (at 5.3 m) within the burn block. The tower placements were carefully chosen to capture the impact of both head and flank fires on the mean and turbulent flows. The hypothesis is that fire-induced perturbations in the lower atmosphere, quantified through parameters like turbulent kinetic energy (TKE) and vertical fluxes, would be substantially stronger than those observed in similar wildland fires under less fire-prone atmospheric conditions. While this hypothesis was validated for heat flux and TKE, it did not hold for momentum fluxes or friction velocity. Additionally, the observations failed to confirm the hypothesis that head fires would produce more intense perturbations than flank fires. Given the homogeneity of fuel, terrain and meteorological elements across the burn unit, this underscores the challenge of disentangling the effects of fire type from other natural factors in a real-world setting. Nevertheless, the finding holds promise for improving turbulence parameterizations in fire-behavior and smoke dispersion models.

1. Introduction

The escalating impact of wildland fires, amplified by the effects of climate change, has raised significant concerns regarding their scale and destructiveness across much of the western US and around the world. The shift towards longer fire seasons and larger fires, propelled by increased fuel availability and atmospheric aridity, has been widely documented (e.g., Abatzoglou and Williams, 2016; Zhong et al., 2021). While there is a wealth of research into climate change impacts on wildfires (e.g., Balch et al., 2017; Liu et al., 2017; Halofsky et al., 2020), the dynamics of fire-atmosphere interactions remains inadequately understood (Clements et al., 2019; Desai et al., 2022). In light of the evolving wildfire landscape and amplified climate change-related risks, there is an urgent need to gain a more comprehensive understanding of fire-atmosphere interactions (Hiers et al., 2020). This knowledge is pivotal in augmenting preparedness and increasing resilience in ecosystems, communities, and firefighting strategies.

Wildland fires hold the potential to reshape the local atmospheric environment, thereby affecting fire behavior through fire-atmosphere interactions (Potter 2002; 2012; Sun et al., 2009). These interactions arise primarily from combustion heat release, which results in convection into the lower atmosphere, giving rise to organized updrafts as strong as 40–60 m s^{-1} extending from the surface to mid troposphere and the potential formation of pyrocumulus clouds (Fromm et al., 2010; Rodriguez et al., 2020; Peterson et al., 2021). The intense heat and the rapid vertical air movement can also lead to the development of fire swirls or whirls, also known as fire vortexes (Forthofer and Goodrick, 2011; Ahmad et al., 2023). These swirling columns of flames and smoke bear resemblance to tornadoes, and on occasion, they manifest as actual tornadoes (Forthofer, 2019; Lareau et al., 2022). The rapidly rising air

* Corresponding author at: Department of Geography, Environment and Spatial Sciences, Michigan State University, 673 Auditorium Rd., East Lansing, MI 48824, USA.

E-mail address: szhong@msu.edu (S. Zhong).

https://doi.org/10.1016/j.agrformet.2024.110000
Received 22 January 2023; Received in revised form 12 March 2024; Accepted 5 April 2024

interacts with cooler ambient air to produce strong downdrafts capable of driving the fire in various directions, contributing to erratic fire behaviors (Lareau et al., 2022).

The rapid fluctuations in wind speed and direction associated with intense heat are conducive to significant turbulence production (Sun et al., 2009; Finney et al., 2011; Filippi et al., 2018; Clements et al., 2019). This fire-induced turbulence plays a pivotal role in modifying the rate of fire spread (Jonko et al., 2021; Katurji et al., 2022a). In areas characterized by strong turbulence, there is a propensity for rapid fire spread due to increased oxygen supply and heat release during combustion, whereas regions with weaker turbulence often experience a slower spread (Clark et al., 1996; Sun et al., 2009; Finney et al., 2011). Turbulent eddies spawned by these processes can transport burning embers and debris, potentially igniting spot fires at a considerable distance ahead of the main fire front (Lareau et al., 2022). Furthermore, turbulence within the fire's plume contributes to vorticity generation through the stretching and tilting of the plume (Finney et al., 2011). Once initiated, turbulent mixing helps sustain the fire vortex or fire swirl by bringing in fresh ambient air into the air column. Beyond its impact on fire behavior, turbulent eddies also play a pivotal role in smoke transport and dispersion (Heilman et al., 2015). On one hand, turbulence facilitates the thorough mixing of smoke plumes with the surrounding clean air, resulting in the dilution of smoke concentrations and the mitigation of local air pollution concerns. Conversely, turbulent mixing also propels smoke particles to higher altitudes, enabling their transport over extended distances, thereby posing potential implications for air quality in regions far from the smoke source (Peterson et al., 2018; Kiefer et al., 2020).

While fire-induced turbulence has been studied in laboratory settings (e.g. Dupuy, 1995; Kuwana et al., 2008) and through numerical simulations (Clark et al., 1996; Sullivan, 2009; Filippi et al., 2018; Zhang et al., 2023), the importance of comprehensive field measurements cannot be overstated, as they provide data in the actual environmental conditions where wildland fires occur (Hiers et al., 2020). However, these field experiments come with challenges related to safety, logistics and instrumentation (Clements et al., 2007, 2019; Seto et al., 2013). To surmount these hurdles, several wildland fire field experiments have effectively combined in-situ and remote sensing technologies to collect valuable real-world data during wildland fires. Prominent examples of such wildland fire field experiments include the grassfire experiments in Southeast Texas (Clements et al., 2007, 2019) and California (Seto and Clements, 2011; Clements and Seto, 2015) of the U.S., the Mediterranean shrub fire experiment in South Corsica France (Morandini et al., 2006), the crop stubble fire experiments near Darfield New Zealand (Finney et al., 2018), a series of low-intensity fires in forested and in grass/shrub environments in Florida and Georgia of the U.S. (Ottmar et al., 2016), and a series of low-intensity prescribed fires in forest understory in New Jersey of the U.S. (Heilman et al., 2015, 2019, 2021a; Clark et al., 2020). These field experiments have played a crucial role in validating various coupled atmosphere-fire behavior models and advancing our understanding of how the feedbacks between fire and atmosphere help shape fire behavior. For instance, data from FireFlux (Clements et al., 2007) have been instrumental in evaluating and improving the WRF-SFIRE model (Kochanski et al., 2013) and the ForeFire-Meso-NH model (Filippi et al., 2013). Additionally, these data have enabled analysis of turbulence generated by different types of fires under diverse environmental conditions (Seto et al., 2013; M. Katurji et al., 2022). However, despite these advances, our understanding of fire-induced turbulence remains limited, especially concerning intense wildland fires under conditions that do not confirm to the controlled criteria of prescribed burns (Heilman 2021b).

In this paper, we focus on the influences of an intense grassfire on turbulence in the atmospheric surface layer, which comprises the lowest 10 % of the atmospheric boundary layer and extends typically from 10 m to 100 m above the Earth's surface depending on atmospheric and surface conditions (Stull, 1988). Specifically, the study is aimed to quantify changes in turbulent flow properties caused by a line fire spreading with the ambient wind through an instrumented micrometeorological flux tower array. Notably, the fire event took place under a Red Flag Warning that signifies weather conditions associated with heightened wildfire risk, making it one of the most intense experimental grass fires ever monitored by flux towers. It is reasonable to hypothesize that wildland fires occurring in more fire-prone atmospheric conditions would exert a greater impact on the ambient atmosphere. The central question we seek to address pertains to the extent of fire-induced turbulence, as quantified by parameters like turbulent kinetic energy (TKE) and vertical turbulent fluxes, and how these characteristics compare with those observed in wildland fires of similar type under less fire-prone atmospheric conditions. The results of this study can lead to improved understanding on how fire-induced turbulence can influence the transport of momentum and scalars between the surface fire and the ambient atmosphere. The knowledge can be used for developing new or improving existing turbulence parameterizations in fire behavior and smoke dispersion models (e.g., QUIC-FIRE, Linn et al., 2020; WRF-FIRE, Coen et al., 2013; WRF-SFIRE, Kochanski et al., 2013; ARPS-FLEXPART, Kiefer et al., 2020).

2. Data and method

The data used in this analysis is from the FireFlux II Experiment conducted on a 40-ha tall grass prairie in La Marque, Southeast Texas on January 30, 2013 (Clements et al., 2019). The fuel type of the experiment site primarily consisted of dried native grass species, such as big bluestem (Andropogon gerardi), little bluestem (Schizachyrium scoparium), and long-spike tridens (Tridens strictus). The fuel loading for the site ranged from 0.41 kg m^{-2} to 0.81 kg m^{-2}, with an average of 0.64 kg m^{-2}. On the morning of the burn, the average fuel moisture content across all sampled vegetation types was recorded at 14 %. The fuels consumption was 90–95 % over the 46 destructive clip plots.

At the moment of ignition, which occurred at 15:04:08 Local Standard Time (LST, 6 h behind Universal Time Coordinated or UTC), the ambient surface air temperature was 15.6°C, relative humidity (RH) was 23.3 %, and the winds were west-northwesterly between 8 and 9 m s^{-1}, occasionally gusting up to 20 m s^{-1}. These conditions, characterized by exceptional dryness and brisk winds, prompted the issuance of a Red Flag Warning by the National Weather Service covering the region of southeast Texas. A Red Flag Warning serves as a vital weather advisory, designed to notify both the general public and firefighting agencies of specific weather conditions associated with an elevated risk of wildfire ignition and rapid spread. The criteria for issuing such warnings may vary between regions, but, in general, they involve a combination of high temperatures, low relative humidity, typically below 20–25 %, and strong winds exceeding 8–11 m s^{-1} or 20–25 miles per hour (mph). Additional factors taken into account include the state of vegetation and fuels, as well as recent weather patterns. Consequently, data collected during this prescribed fire experiment provided a rare opportunity to observe potential changes to turbulent flows by grass fires occurring under fire-prone atmospheric conditions that have been deliberately avoided during prescribed wildland fire experiments.

The experimental design consisted of a number of different instrument platforms and sensor systems. A suite of four meteorological towers were aligned in a diamond formation to collect high frequency samples of wind and temperature as the fire spread across the burn block (Fig. 1). A permanent 43-m tall tower, referred to as the main tower (MT), was located in the northern portion of the burn block and three additional 10-m short steel towers were positioned to the southeast (referred to as Short Tower East, STE), southwest (Short Tower West, STW) and south (Short Tower South, STS) of the main tower, comprising the diamond formation (Fig. 1).

This study focuses on the data collected using three-dimensional (3D) sonic anemometers (Applied Technology, Inc., ATI) mounted at three levels (20, 10, and 5.8 m) on the main tower and at a single level

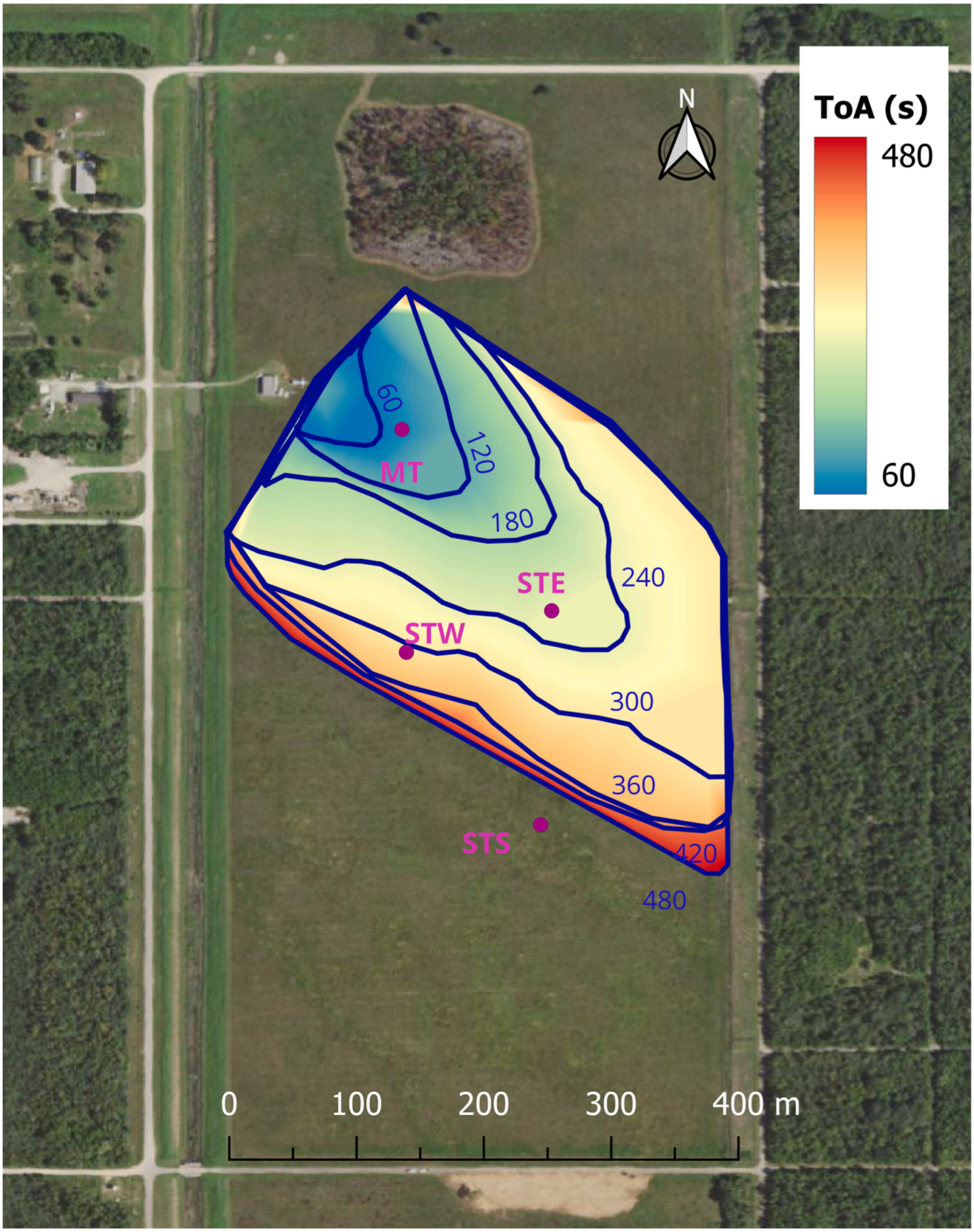

Fig. 1. The burn block and positions of the 43-m main tower and the three 10-m short towers. The blue line contours are fire perimeters determined from the tower-mounted and airborne infrared cameras. Magenta circles indicate tower positions, with MT denoting the main tower, and STE, STW and STS denoting short towers located to the east, west and south of the main tower, respectively. The shading indicates the time of the fire front's arrival measured in seconds since ignition.

(5.3 m) on the short towers. The 5.3-m level on the short towers did not precisely align with the lowest level of 5.8 m on the main tower. This discrepancy arose from variations in the base plate and mounting configurations between the main and short towers. The 3D sonic anemometers recorded east-west (u), north-south (v), and vertical (w) wind velocity components and sonic temperatures with a sampling rate of 10 Hz.

Using images from infrared (IR) cameras mounted on the main tower and on a helicopter flying 400–500 m above the burn block, the fire front perimeters (blue contours in Fig. 1) were estimated and were used to subjectively determine if the towers were under the influence of a head fire (fires that burn or spread with prevailing wind) or a flank fire (fires that burn or spread perpendicular to the prevailing wind). The ignition was started as a line fire along the northwestern boundary of the burn block, which then spread with the ambient wind rapidly through the tower array in the burn block (Fig. 1). As the fire front spread towards

MT, the head of the fire narrowly missed a direct impact on the tower. However, for the analysis here, MT is considered as impacted by a head fire. The fire then continued to spread towards STE, affecting it as a head fire, and the STW with its right flank. Although STS is located outside the perimeter of the IR images due to its position, based on the evolution of the fire it becomes evident that it was impacted by the head fire. The average head-fire rate of spread, estimated based on the IR images, was approximately 1.6 m s^{-1}, while the flank-fire propagation was between 0.8 and 0.96 m s^{-1}, and the maximum IR temperature approached 900 °C.

The comprehensive details of the experimental setup, including instrument specifications and calibration procedures, can be found in Clements et al. (2019). Notably, the ATI sonic anemometers underwent custom calibration up to 350 °C by the manufacturer. Furthermore, laboratory tests employing high-temperature heat guns were conducted. Co-located fine-wire thermocouples alongside the sonic anemometers recorded peak temperatures of approximately 350 °C within the lowest 5 m of the plume during fire front passage. Following the experiment, a field intercomparison among all sonic anemometers was carried out on-site, revealing that they operated within their anticipated performance parameters.

The data from the sonic anemometers at each tower were rotated from Cartesian to streamline coordinate and tilt-corrected following Wilczak et al. (2001). The longitudinal, lateral and vertical velocity

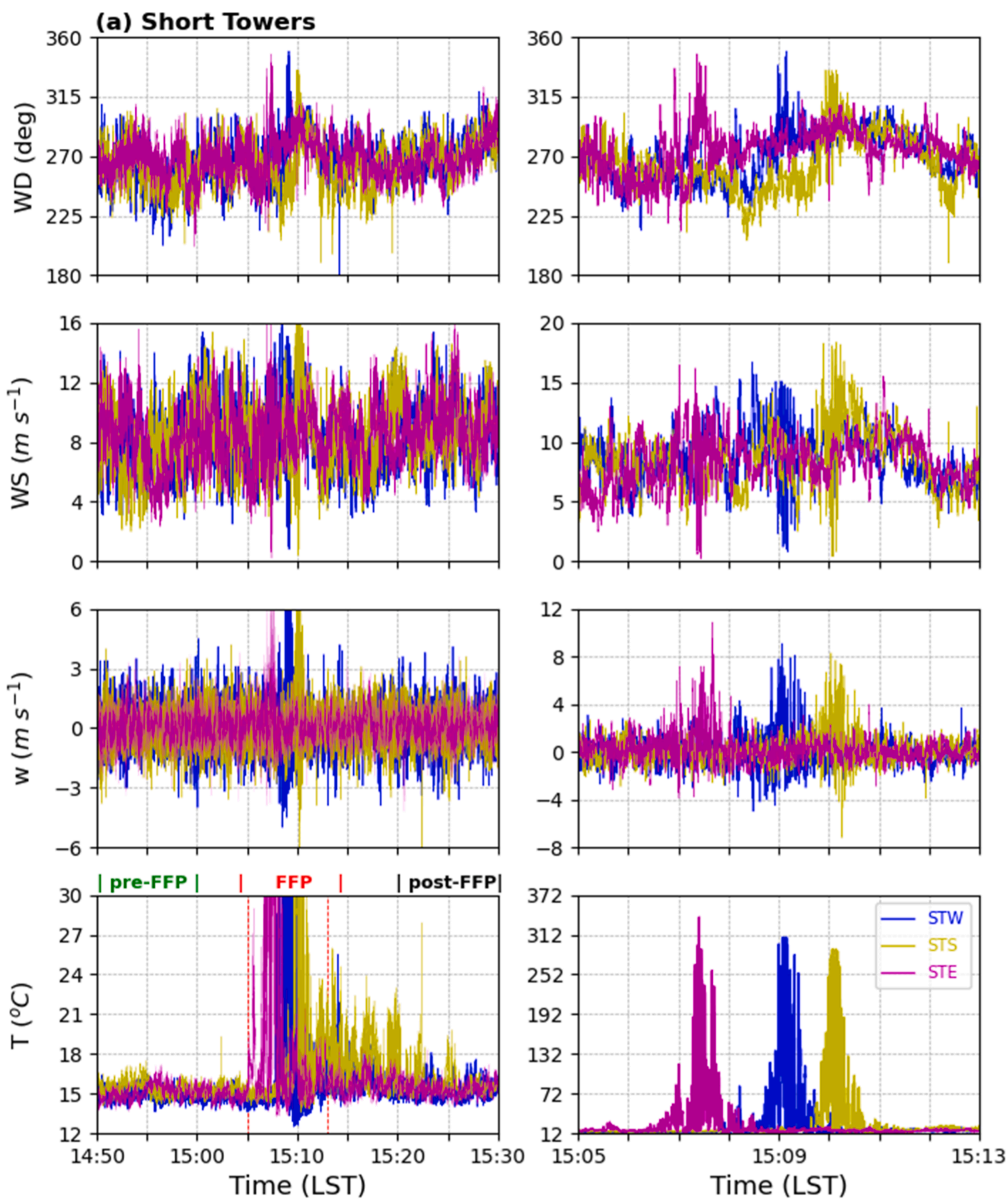

Fig. 2. Observations of 10-Hz horizontal wind direction (top), wind speed (second from top), vertical velocity (second from bottom) and temperature (bottom) at the three short towers (a) and the main tower (b). The right panel provides a closer view of the time period highlighted by the two red vertical dashed lines in the lower left panel. .

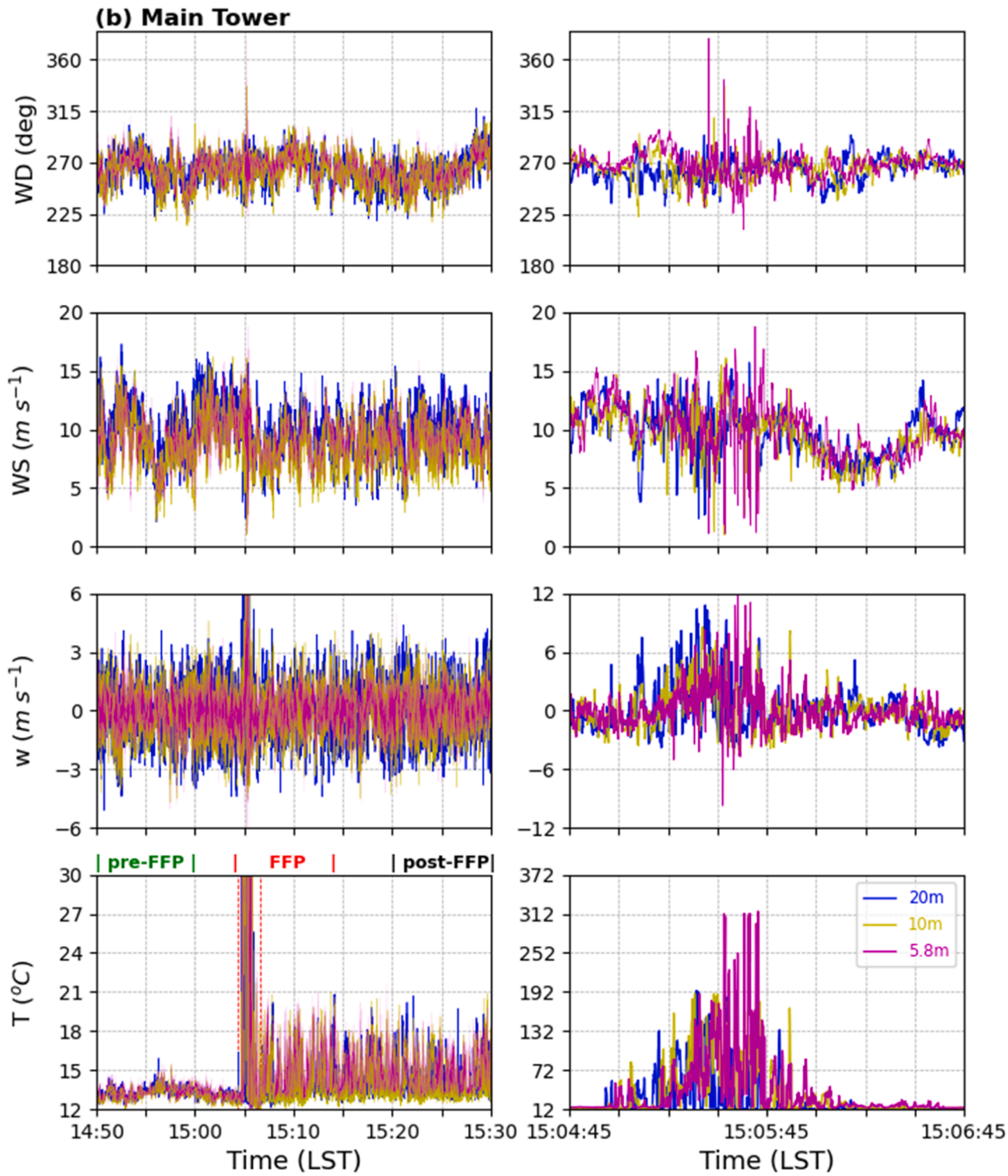

Fig. 2. (*continued*).

perturbations ($u^{'}$, $v^{'}$, $w^{'}$) and temperature perturbations (T') were calculated by subtracting 10-min block-averaged means ($\overline{u}, \overline{v}, \overline{w}, \overline{T}$) from the 10-Hz data. In line with the methodology described by Seto et al. (2013, 2014) and Heilman et al. (2015, 2017, 2019, 2021a), the current analyses incorporated the practice of replacing the means calculated for the fire period with those from the period preceding the fire. This adjustment was made to ensure an accurate representation of the turbulence generated by the fire. Further elaboration on this approach, along with the rationale for selecting 10-minute block averages for representing the mean flow characteristics, will be provided in greater detail in the forthcoming Discussion section.

The results below is organized as follows. It begins by showing original velocity and temperature time series as the fire front progressed through the tower array. It then delves into an analysis of the fire-induced turbulent heat and momentum fluxes as well as turbulent kinetic energy. The section ends with a discussion on the alteration in velocity distribution or turbulence regime prompted by the fire front. Of particular note is the revealing of the fire front's impact through comparisons of various quantities before, during and after its passages. The height dependency of the fire influence is elucidated by comparing observations at the 5.8, 10 and 20 m levels on the main tower. Spatial variations and the influence of fire type (head fire vs. flank fire) are further explored through comparisons of observations at the three short towers and the lowest level on the main tower.

3. Results

3.1. Fire-induced changes to temperature and velocity

Fig. 2 shows the time series of the 10-Hz temperature, horizontal wind speed and direction, and vertical wind component between 14:50 LST and 15:30 LST on the day of the fire. It is important to note that the temperature referred to is the sonic air temperature. The line fire was ignited along the northwestern boundary at 15:04:08 LST swiftly spreading with the prevailing northwesterly ambient winds across the tower array. As indicated by the sharp rise in temperature, the fire front first impinged on MT at 15:05:27 LST, followed by STE at15:07:24, STW at 15:09:08 and finally STS at 15:10:08 LST. Based on the time when the fire reached the first tower (MT) and the time when it passed the last tower (STS) in the tower array, three 10-min time periods were identified to highlight fire front passage or FFP (15:04 – 15:14), pre fire front passage or pre-FFP (14:50–15:00) and post fire front passage or post-FFP (15:20–15:30). These periods were applied consistently to all the towers, although the exact moment when the fire was first detected by the instrument on each tower varied. It is important to highlight that there were distinct intervals between each of the three periods, separated by several minutes. This deliberate decision to create non-overlapping periods served the purpose of reducing the risk of contamination from the passage of the fire front on the periods preceding and following its occurrence. By adopting this approach, our objective was to guarantee that the mean values calculated during the pre-FFP period accurately represent the ambient conditions unaffected by the fire, while the values during the post-FFP period accurately reflect conditions not directly influenced by the fire front.

Despite the differences in their locations relative to the fire front, the magnitude and variation of the instantaneous temperature, wind speed and wind direction at the three short towers were similar (Fig. 2a). The time series at these towers showed significant degree of overlap prior to the arrival of the fire front, suggesting spatially uniform ambient atmosphere across the burn block (Fig. 2a). Prior to the arrival of the fire front, the minimum temperatures detected by the towers varied between 13 °C at STW and 15 °C at STE while the maximum temperatures ranged from 16 °C at STW to 19 °C at STE. The fire front drastically increased temperature from the ambient values of less than 20 °C to peak values ranging from 290 °C at STS to 340 °C at STE. Immediately following the fire front passage, the temperature sharply dropped to values below the pre-FFP level before returning to a general post-FFP level (Fig. 2a). The sharp dip in temperature behind the fire front was transient, lasting about 1 min, and the transition from the ambient temperature to the peak value and back occurred within 10 min. The distribution around the peak exhibited some asymmetry, with average post-FFP temperature 2–3 °C higher than that during the pre-FFP period. In addition to higher values, the post-FFP temperature variance was also substantially larger compared to the pre-FFP period. This asymmetry between the pre-FFP and post-FFP was expected, as heat from the fire meandered around the burn block following the FFP, although a small portion of the differences may have been a result of diurnal temperature variations. The peak temperature perturbation was higher at STE (affected by head fire) than at STW (influenced by flank fire), suggesting more intense heating associated with the head fire than the flank fire. This, however, was not corroborated by the fact that the peak temperature value at STS (also hit by head fire) was somewhat lower than that of STW (Fig. 2a). This difference in the comparisons between STW situated on the path of the flank fire with the two other short towers (STE and STS) influenced by the head fire underscores the challenge of isolating the effects of fire type (head vs. flank) on air temperature in a real-world situation.

The time series of instantaneous vertical velocity at the three short towers during the pre-FFP and post-FFP periods display sporadic variations with both upward and downward motions, each generally remaining within the range of less than 5 m s^{-1} and centered around a near-zero mean (Fig. 2a). Corresponding to the 20–30 fold rise in temperature during the FFP was a sudden surge in the vertical motion, with maximum instantaneous updrafts ranging from about 8 m s^{-1} at STS to 11 m s^{-1} at STE. While there was an increase in downward motion as well, the downdrafts were less intense than the updrafts (Fig. 2a). It is noteworthy that the peak updraft speed occurred slightly after the peak temperature.

Interestingly, the asymmetry in temperature variance between the pre-FFP and post-FFP periods was not observed in vertical velocity. Vertical motions during the post-FFP period appeared to fluctuate at levels similar to those observed during the pre-FFP period despite the increased instability in the surface layer during post-FFP caused by residual surface heating (Fig. 2a). Moreover, the strength of the peak updraft at STW, influenced by the flank fire, was between the strengths observed at the two towers affected by the head fire, making it difficult to draw any conclusion about how fire type might affect the intensity of vertical motion.

Compared to the alterations in instantaneous temperature and vertical velocity, fire-induced changes to wind direction and speeds were relatively small at the three short towers. The instantaneous wind speed fluctuated in the range of 2–16 m s^{-1} during the pre-FFP period, which expanded to 0.5–18 m s^{-1} during the FFP period (Fig. 2a). Wind directions were generally westerly during the pre-FFP period, becoming highly variable during the FFP period, varying between southwesterly and north-northwesterly, indicating an increase in lateral wind component as ambient air was drawn towards the fire front. Wind speed fluctuations were slightly smaller during the post-FFP compared to the pre-FFP, possibly due to the reduction in roughness lengths by the burn (Fig. 2a).

In contrast to the relatively small horizontal variations in the observed temperature and velocity, as indicated by the three short towers, there were substantial variations between the three vertical levels on the main tower and the variations are larger between the 5.8 m and the 10 m levels than between the 10 m and 20 m levels (Fig. 2b). A sharp rise in temperature associated with the FFP occurred at all three levels, peaking slightly earlier at the two upper levels, which is indicative of the forward tilt of the thermal plume with height. The heating from the surface fire decreased rapidly from a peak temperature of more than 310 ^{o}C at 5.8 m to approximately 190 ^{o}C at the 10 m and 20 m levels (Fig. 2b). The noteworthy aspect here is the non-linear decrease with height above ground in atmospheric heating by the fire, with the majority of this decrease observed below the 10-meter level. In contrast, velocity perturbations, whether vertical or horizontal, exhibited similar magnitude at all three levels, although noticeable changes in direction were more pronounced at the lowest level (Fig. 2b). The magnitudes of the FFP-induced temperature and velocity perturbations at the 5.8 m level (Fig. 2b) were comparable to those observed at the 5.3 m level on the short towers, particularly at STE (Fig. 2a).

In summary, the FFP was associated with a rapid and substantial temperature surge, peaking at over 300 °C at 5.8 m, with a subsequent swift decline to less than 200 °C at 10 and 20 m. The FFP was also related to significant updrafts exceeding 10 m s^{-1}, accompanied by somewhat weaker downdrafts. The vertical velocity perturbations were slightly more intense at 5.8 m than at 10 m or 20 m. Compared to the pre-FFP period, the post-FFP period was characterized by higher mean temperature and increased temperature variability, likely attributed to a combination of heat meandering on the ground from smoldering activities and the diurnal temperature fluctuations. In contrast, velocity variability slightly decreased during the post-FFP period, possibly resulting from reduced roughness due to the burn. Furthermore, peak perturbation temperatures and vertical velocities observed at STW, influenced by flank fires, were lower than those at MT and STE, but comparable to those at STS, all of which were influenced by head fires. This inability to substantiate the hypothesis that perturbations are generally more intense under head fires than flank fires highlights the challenge of isolating the effects of fire type on fire-induced perturbations in a real-world setting.

3.2. Fire-induced changes to turbulent heat and momentum fluxes

The 10-s averaged vertical turbulent heat fluxes, $\rho C_p \overline{w'T'}$ (ρ is ambient air density and C_p is heat capacity), during the pre-FFP period were relatively uniform and small, with values generally less than 1 kW m^{-2}across the three short towers (Fig. 3a). The heat release from the fire and the increased vertical velocity perturbation (Fig. 2a) led to a drastic increase in upward vertical turbulent heat flux during FFP, reaching nearly 400 kW m^{-2} (Fig. 3a). The heat flux continued to fluctuate between -1 kW m^{-2} and 6 kW m^{-2} during post-FFP, while the amplitude of fluctuations decreased with time and eventually approached the pre-FFP level near the end of the post-FFP. The behavior of turbulent heat fluxes, including the peak values, appeared to be independent of the location of the towers on the path of the fire front, as indicated by the resemblance in the heat flux observations at STW and STS. In other words, no significant difference was found in turbulent heat fluxes between the tower hit by head fire (STS) and the tower influenced by flank fire (STW). It is worth noting that the 10-s averaged peak heat flux at STE was approximately 50 kW m^{-2} less than that at STW and STS (Fig. 3a), although the peak instantaneous temperature and vertical velocity during FFP were higher at STE than at STW and STS (Fig. 2a). A closer look revealed that the peak vertical velocity perturbation

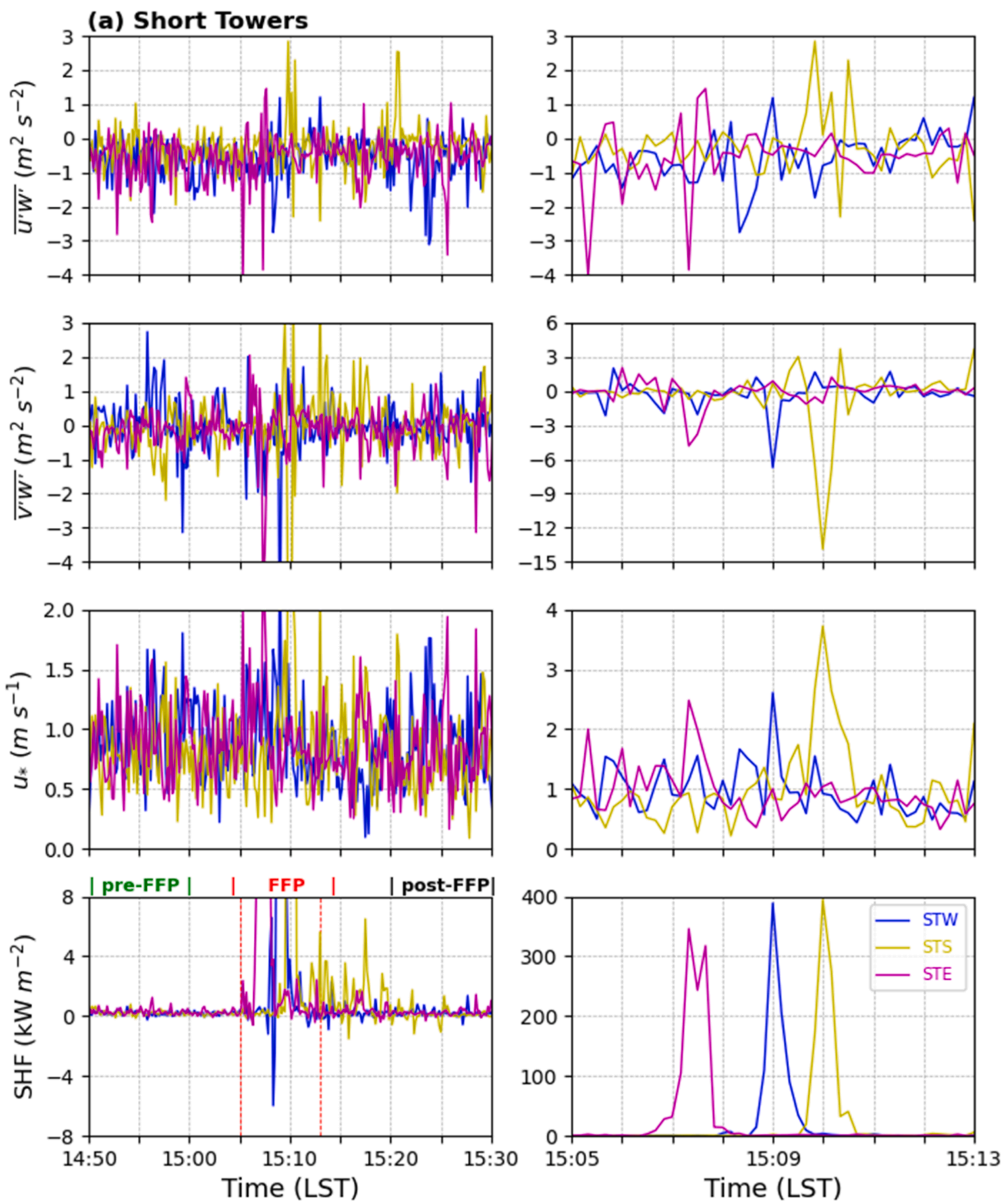

Fig. 3. Observations of 10-second averaged longitudinal (top) and lateral (second from top) component of vertical fluxes of horizontal momentum, friction velocity (second from bottom) and heat flux (bottom) at the three short towers (a) and the main tower (b). The right panel provides a closer view of the time period highlighted by the two red vertical dashed lines in the lower left panel.

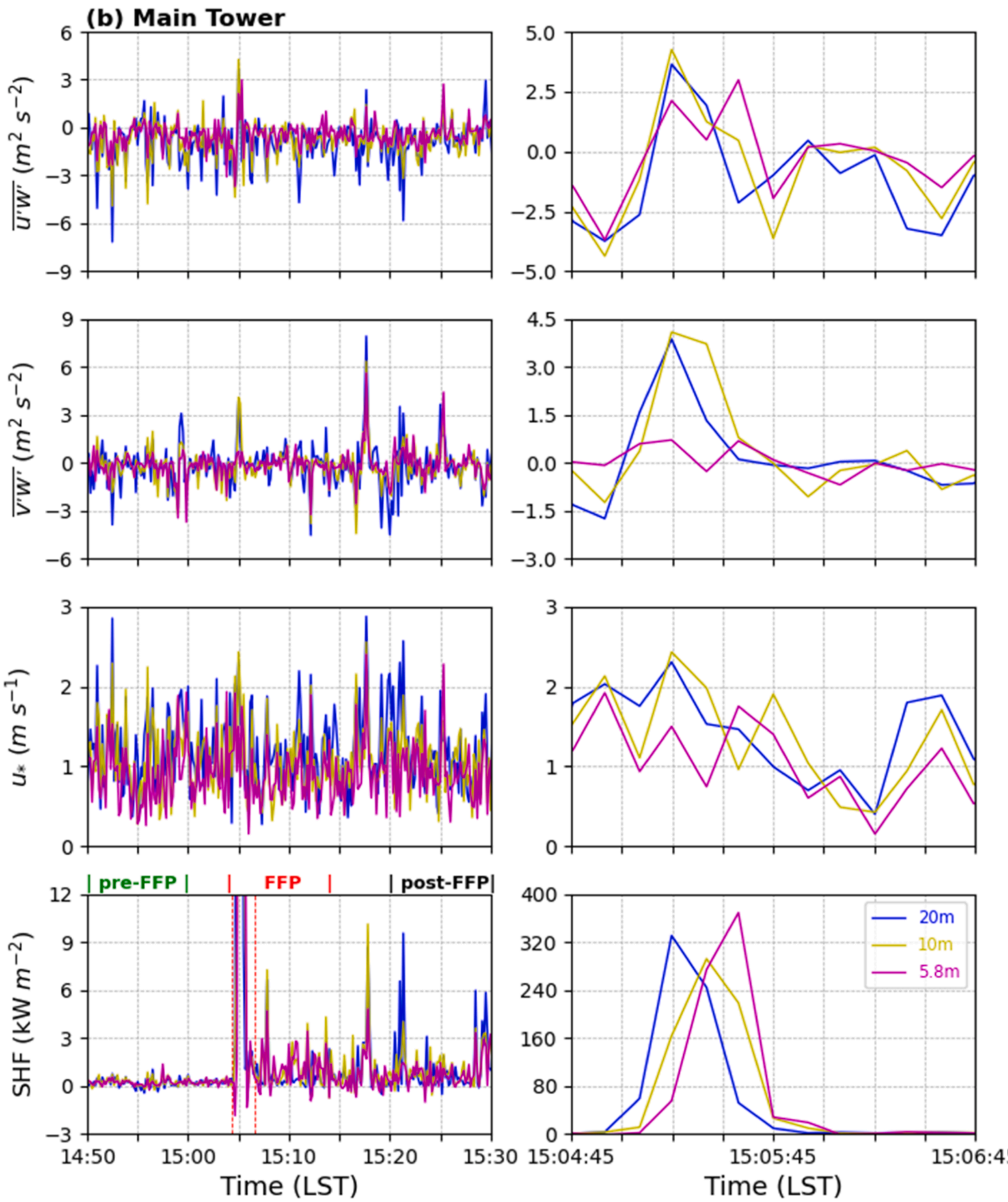

Fig. 3. (*continued*).

occurred shortly after the peak temperature perturbation at STE, whereas at the two other towers, these peaks were more synchronized (Fig. 2a).

The 10-second averaged vertical fluxes of horizontal momentum at the three short towers (Fig. 3a) were dominated by the longitudinal component, $\overline{u'w'}$, during the pre-FFP period. The predominantly negative momentum fluxes indicated a downward transfer of higher momentum air, as expected from the increase of wind speed with height. The FFP period was characterized by an increase in both the longitudinal and lateral components of vertical momentum fluxes. The increase in the two components were comparable at STE, while at STW and STS, the increase in the lateral momentum flux component was much larger than that of the longitudinal component. Worth noting, was the increase in the positive longitudinal momentum fluxes during the FFP, suggesting higher momentum air in the combustion zone being transferred upward by turbulent eddies. The friction velocity, denoted as $u_* = (\overline{u'w'}^2 + \overline{v'w'}^2)^{1/4}$and serving as a measure of the magnitudes of the vertical fluxes of horizontal momentum, increased by 25 %-200 % from under 2 m s^{-1} at all three towers during the pre-FFP period, to between 2.5 and 4 m s^{-1} during the FFP period (Fig. 3a). Although the lateral momentum flux component reached its absolute maximum during FFP, the longitudinal momentum flux component exhibited peaks during post-FFP (e.g., the peaks around 15:21, 15:24 and 15:26 LST at STS, STW and STE, respectively) were comparable to the peaks observed during the FFP period (Fig. 3a).

The observations at the main tower (Fig. 3b) showed a systematic increase with height in both the magnitudes and the range of fluctuations of friction velocity and the longitudinal momentum flux component, a feature expected from increased wind speed with height. However, the peak heat flux exhibited a decrease from 5.8 m to 10 m, but a slight increase from 10 m to 20 m (Fig. 3b). At all three levels, the FFP was associated with only a local maximum in the momentum flux and friction velocity. The absolute maximum of lateral momentum flux component and friction velocity were observed between 15:17 and 15:18 LST during the post-FFP period, and the absolute maximum for the longitudinal component was recorded between 14:52–14:53 LST during the pre-FFP period (Fig. 3b). However, the peaks in heat flux during the FFP period were orders of magnitudes larger than the peaks during the pre-FFP and post-FFP periods. At nearly 400 kWm^{-2}, the fire-induced maximum heat flux at the lowest level (5.8 m) on the MT (Fig. 3b) was similar to the peak values observed at 5.3 m on the three short towers (Fig. 3a).

3.3. Fire-induced changes to turbulent kinetic energy

Turbulent kinetic energy (TKE), defined as $\frac{1}{2}(\overline{u'^2} + \overline{v'^2} + \overline{w'^2})$, where $\overline{u'^2}$, $\overline{v'^2}$ and $\overline{w'^2}$ are longitudinal, lateral and vertical velocity variance and the overbar indicates 10-s average, is commonly used as a measure of turbulent intensity and is widely used to parameterize turbulent transfer in atmospheric boundary layer in many atmospheric dispersion models including models used to predict fire smoke dispersion (Kiefer et al., 2020). As shown in Fig. 4, the FFP was marked by a single, distinct peak in vertical velocity variance at all three short towers (Fig. 4a) and across all three levels on the main tower (Fig. 4b). At STS, the FFP coincided with an absolute peak in the variance of the two horizontal velocity components, which in combination with the absolute peak in vertical velocity variance, yielded a pronounced TKE maximum of approximately 40 $m^2\ s^{-2}$ (Fig. 4a). However, at STW and STE, the peak TKE values during FFP, about half the peak value at STS, were akin to the peaks observed outside the fire period. These TKE peaks occurring outside the fire period were attributed to the absolute peaks in the longitudinal velocity variance observed around 15:26 LST during post-FFP period at STE and approximately 14:59 LST during pre-FFP period at STW (Fig. 4a). These findings suggest that while fire induces a surge in vertical velocity variance, the fire-induced peaks in horizontal velocity variance are comparable to those that occur in daytime boundary layer under windy conditions.

No discernible systematic differences in the velocity variance and TKE were evident between the pre-FFP and post-FFP periods (Fig. 4a). The similarity between STE and STW suggested that the type of fire had little influence on velocity variance and TKE.

A similar evolution pattern of velocity variance and TKE was observed at the three levels on the MT (Fig. 4b). In contrast to the FFP-induced peak in the vertical fluxes of horizontal momentum, which increased slightly with height, the FFP-associated TKE peak exhibited a slight decrease with increasing height (approximately 20, 19, and 18 $m^2\ s^{-2}$ at 5.8, 10 and 20 m, respectively). This divergence arose from the variance of the two horizontal velocity components decreasing with height, even as vertical velocity variance increased with height (Fig. 4b).

Similar to the short towers, the peak TKE values during the FFP period at all three levels on the MT were akin to those observed outside the fire period. Notably, an absolute TKE peak of about 25 $m^2\ s^{-2}$ was registered at the 10-meter level, occurring around 15:21 LST during the post-FFP period, which was due primarily to a surge in the lateral velocity variance.

The relative contributions to TKE from horizontal and vertical velocity variance, measured by the ratio, $\overline{w'^2}/(2 \times TKE)$, reveals the level of anisotropy in turbulence regimes. If this ratio is less than 1/3, TKE is dominated by horizontal velocity variance and the turbulence is anisotropic. A ratio close to 1/3 suggests isotropic turbulent regime (Heilman et al., 2015).

The pre-FFP ratios were well below 1/3 at 5.8 m on the MT and the three short towers (Fig. 5), indicating anisotropic turbulence. This outcome was anticipated due to the proximity to the ground surface,

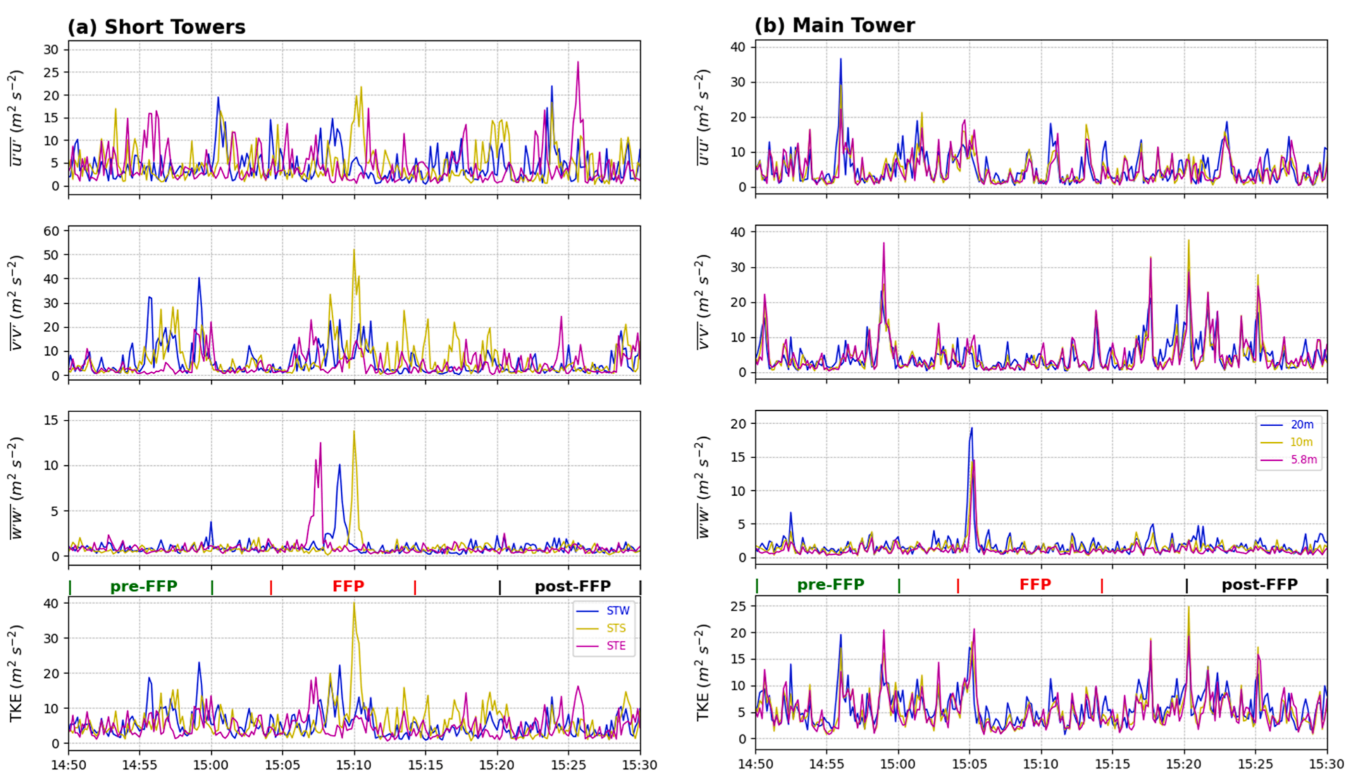

Fig. 4. Observations of 10-second averaged longitudinal (top), lateral (second from top) and vertical (second from bottom) velocity variance and turbulent kinetic energy (bottom) at the three short towers (a) and the main tower (b). .

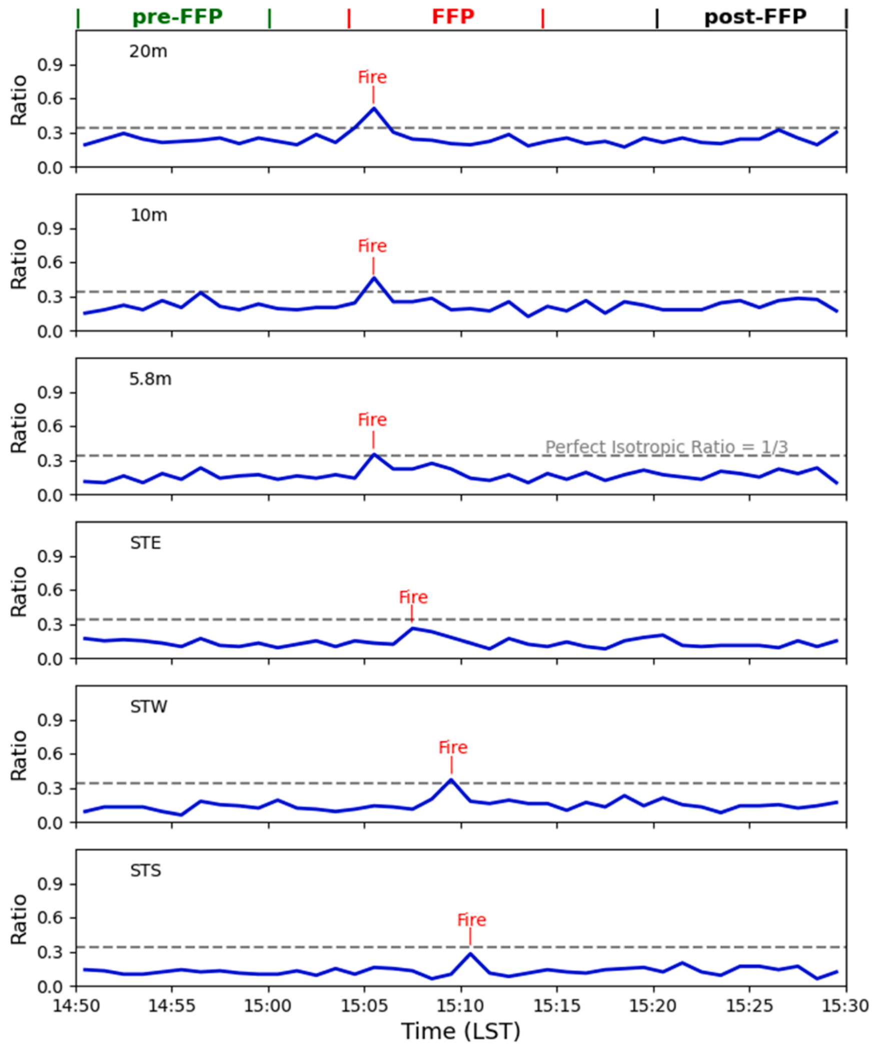

Fig. 5. Observations of 1-minute averaged ratios of vertical velocity variance to the sum of longitudinal, lateral and vertical velocity variance at the main tower and the three short towers.

where the vertical component of turbulent motion was dampened, and consequently, an anisotropic turbulence regime is expected (Fig. 5). The ratios were larger higher up at 10 m and 20 m than at 5.8 m on the MT, but still below 1/3, except for a few isolated moments (Fig. 5). The ratios during FFP increased to near 1/3 at 5.8 m and to above 1/3 at 10 m and 20 m, indicating that the effect of FFP was to move turbulence field toward isotropy or toward a turbulence regime more heavily influenced by vertical velocity variations. At 20 m, the ratio was greater than 0.5, suggesting that the TKE became dominated by the vertical velocity variance due to the fire. The observations at the three short towers closely resemble that at the lowest level on the MT.

3.4. *Fire-induced changes to velocity distribution*

Changes to the turbulent velocity distributions by the fire can be measured by Skewness (S) and Kurtosis (K) computed as normalized third-order and forth-order moments, respectively. A turbulence velocity distribution with $S = 0$ or $K = 3$ is a Normal or Gaussian distribution and a non-zero value of S or K-3 suggest a departure from the Gaussian regime (Wilson and Flesch, 1997).

During the pre-FFP period, both the horizontal and vertical velocity distributions were nearly Gaussian with S values varying between ± 0.15 (except for STW with $S = 0.3$) and $|K - 3| < 1$ (Figs. 6, 7). The horizontal velocity distribution remained nearly Gaussian during the FFP and Post-

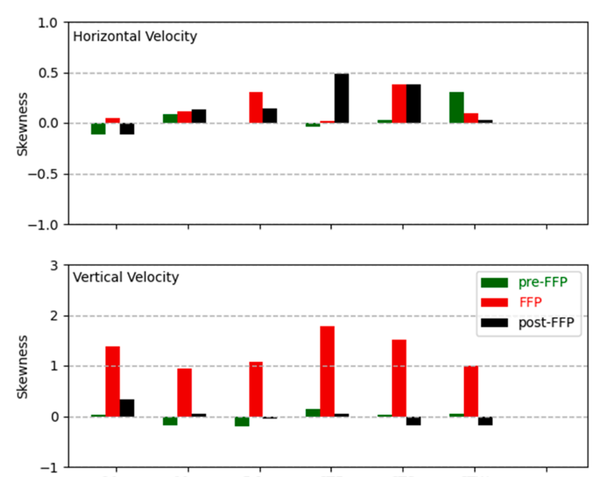

Fig. 6. Skewness of the horizontal (top) and vertical (bottom) velocity perturbations at the three short towers and the main tower during pre-FFP, FFP and post-FFP.

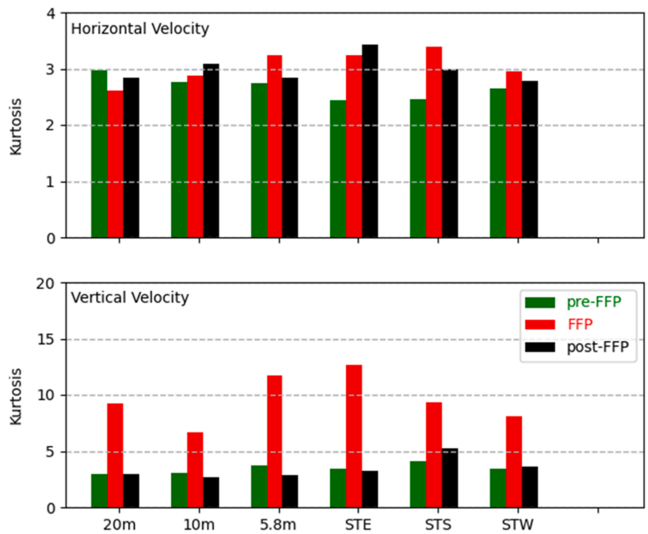

Fig. 7. Kurtosis of the horizontal (top) and vertical (bottom) velocity perturbations at the three short towers and the main tower during pre-FFP, FFP and post-FFP.

FFP periods. However, the vertical velocity distributions during the FFP exhibited significant departure from Gaussian, with $1 < |S| < 3$ and $6 < |K - 3| < 36$ among the towers (Figs. 6, 7). The large, positive S and K for vertical velocity suggested the presence of stronger, narrower updrafts surrounded by weaker, broader downdrafts during FFP. This asymmetry in the updrafts and downdrafts associated with FFP has important implications for scalar (smoke particles, heat and moisture) transport into and out of the combustion zone in the atmospheric boundary layer. However, operational dispersion models often rely on diffusion parameterizations that assume Gaussian turbulence. Given the observed asymmetry in the updrafts and downdrafts associated with fire front, it is likely that these models may produce inaccurate predictions of smoke distribution.

4. Discussion

In comparison to previous wildland fire experiments, the turbulent perturbations observed during this experiment either exceeded or fell within the upper range of what has been documented previously (e.g., Clements et al., 2008; Seto et al., 2013; Clark et al., 2020; Heilman et al., 2015, 2017, 2019, 2021a; Katurji et al., 2022a). This outcome aligns with expectations, considering the unique characteristics of the fire under examination and the red flag conditions, indicative of fire-prone atmospheric conditions, under which the experiment was conducted. However, it is crucial to exercise caution when comparing the magnitudes of turbulent properties such as TKE and heat and momentum fluxes from our study with those of other experiments, as these values can exhibit substantial variations depending on the chosen averaging time period used in the data analysis.

A fundamental assumption in the analysis of turbulence data is the selection of an averaging time scale for computing the mean flow properties, from which turbulent perturbations or fluctuations are determined as deviations from the mean. For slower burning, low-intensity fires, longer time scales ranging from 10^1 to 10^2 min have usually been applied to compute the means. Conversely, for fast spreading, high-intensity fires, smaller time scales of 10° to 10^1 min have often been employed. The choice of an averaging time scale ultimately defines what constitutes turbulent fluctuations relative to the ambient atmospheric flows surrounding the fire, thereby significantly influencing the interpretation of the analysis results.

Furthermore, the selection of the averaging time scale can also be influenced by the specific research questions being addressed. If the inquiry pertains to the longer-term effects of a fire on the surrounding atmospheric boundary layer, a longer time scale may be preferred. Conversely, if the focus is on capturing short-term variations in wind patterns and their feedback on fire behavior, a shorter time scale may be more appropriate.

Previous studies on atmospheric turbulence observed during prescribed fire experiments have applied a range of time scales for computing means and perturbations. For example, Clements et al. (2008) utilized a 1-minute running average for their analysis of data collected during the FireFlux experiment conducted in 2006 on the same burn plot as this experiment. This choice of a 1-minute running mean is likely to filter out the effects of large eddies resulting from fire-atmosphere interactions, leading to smaller magnitudes of turbulent fluxes. This reduction in turbulence magnitude is expected, as part of the turbulent fluctuations is already represented in the rapidly modified mean flow affected by the fire. Similarly, in an investigation of above-canopy turbulence and energy fluxes during eight prescribed fires in pine-dominated forests of the New Jersey Pinelands, Clark et al. (2020) employed a 1-minute averaging period for deriving TKE. However, they extended the averaging period to 10 min when computing turbulent momentum and heat fluxes. The 10-min averaging period was also selected by Seto and Clements (2011) in their analyses of data collected during prescribed grass fire in a narrow valley.

In contrast, much longer averaging period of 30 min was utilized in Seto et al. (2013) that analyzed data from four prescribed fire experiments characterized by different fuel, terrain, and atmospheric conditions. Additionally, to ensure that the perturbations more accurately represent fire-induced turbulence, they replaced the mean values computed during the fire period with the 30-minute block average from the block immediately preceding the fire period. A similar approach of replacing fire-period mean with pre-fire period mean was adopted in a series of studies conducted by Heilman et al. (2015, 2017, 2019, 2021a) that explored turbulence during low-intensity forest understory fires in the New Jersey Pine Barrens. In our current analyses, we also adopted the approach of replacing the fire-period mean with the pre-fire period mean. This choice allowed us to depict ambient atmospheric flow unaffected by the fire, thereby treating all fire-induced perturbations as turbulence.

In addition to the time period chosen for computing mean flow properties, time period used to average variance (i.e. TKE) and covariance (e.g. turbulent heat and momentum fluxes) also affects the magnitude of these quantities, with longer periods generally yielding lower average values. Some studies applied the same averaging period for computing turbulence perturbations of individual variables and the variance and co-variance of these perturbations (e.g. Clements et al. 2008), while others opted for different averaging periods (e.g., Heilman et al. 2017).

It is worth noting that although the averaging period or the filter length holds significance, the analysis of the statistical population of eddies through Gaussian statistics does not align well with the non-stationary and non-Gaussian nature of our current problem.

Despite the challenges posed by differences in fire characteristics and chosen averaging time scales, as well as the limitations association with employing Gaussian statistics for the analyses, it is important to recognize that comparative analyses across diverse experiments can still provide valuable insights into fire-induced turbulence and fire-atmosphere interactions. Such intercomparisons contribute to our collective understanding of these complex phenomena and their broader implications.

Comparing the results of this study with those from the FireFlux experiment conducted earlier on the same burn plot with similar fuel conditions (Clements et al. 2007, 2008), a striking contrast emerges in terms of turbulent heat fluxes. In this study, peak turbulent heat fluxes were found to be at least an order of magnitude larger, registering approximately 300–400 kW m^{-2}, as opposed to the 25–30 kW m^{-2} recorded in FireFlux. This notable disparity can be attributed, in part, to the different meteorological conditions, as well as to the differing averaging periods employed; the current study adopted a 10-minute block average for computing mean flow characteristics and 10-second averaging period for the fluxes, whereas FireFlux utilized a one-minute running average for both. Nevertheless, based on instantaneous measurements of temperature and vertical velocity, the peak instantaneous heat flux was estimated to reach approximately 3.5 MW m^{-2} in this study, exceeding threefold the peak value of 1 MW m^{-2} recorded during FireFlux. The much larger heat flux during this experiment can be ascribed to the Red Flag Warning condition, characterized by drier fuel conditions leading to increased heat release from combustion, as well as significantly stronger wind speeds during the burn. It is important to highlight that the conversion from the unit (°C m s^{-1}) of kinematic heat flux ($\overline{w'T'}$) to the unit (W m^{-2}) of heat flux ($\rho C_p \overline{w'T'}$) did not consider the alteration in air density induced by the fire, which is expected to be lower than the surrounding ambient air density. As a result, the fire-induced heat flux values are likely overestimated. Besides the differences in the magnitude of the heat fluxes, notable distinction is also found in the vertical distribution of peak heat flux values. In this experiment, the peak fire-induced turbulent heat flux exhibited a decrease from 5.8 m to 10 m, followed by a slight increase from 10 m to 20 m. In contrast, the peak heat flux values observed during FireFlux consistently decreased with increasing height, occurring at 2, 8, 20, and 43 m.

What is particularly intriguing is that the magnitudes of momentum fluxes or friction velocity remain relatively comparable, ranging approximately 3–8 m^2 s^{-2}. This unexpected similarity suggests that during the occurrence of a fire, momentum flux or shear stress is primarily influenced by local and smaller eddies, while heat flux is predominantly governed by larger eddies.

While the velocity covariance or momentum fluxes exhibit similarities between the two studies, noticeable distinctions emerge in the case of velocity variance or TKE, with TKE in the current study approximately twice the values recorded in the FireFlux experiment. It is worth noting that this dissimilarity, though more pronounced than the difference in momentum flux, remains relatively minor when contrasted with the substantial differences in heat flux. This discrepancy can be attributed to the significantly greater influence exerted by the large eddies generated by the fire on temperature and vertical velocity perturbations, as opposed to their impact on horizontal velocity perturbations.

Despite the aforementioned differences, several noteworthy characteristics observed during this experiment mirror those documented in the FireFlux experiment. These commonalities include the forward tilt of the plume with increasing height, the dramatic surge in upward heat flux during the fire, the transition of momentum flux from predominantly downward to upward, and the observation that the peak in TKE and u_* may represent a local maximum, rather than the absolute maximum that might occur prior to or after the fire. In essence, despite the generation of remarkably high heat flux, these grassfires do not yield TKE and shear stress values significantly exceeding those observed in a daytime windy boundary layer. Furthermore, the fire induces a shift in turbulence towards a more isotropic regime, as the vertical velocity variance becomes comparable to the horizontal velocity variance. This stands in contrast to the pre-fire and post-fire conditions when the latter is much larger, representing anisotropic turbulence.

Moreover, the current study sought to differentiate between head fire and flank fire influences. Regrettably, the results do not offer definitive distinctions, highlighting the inherent complexities in delineating their differences in a real world setting. Further research may be warranted to refine this understanding.

5. Conclusions

The in-situ sonic anemometer measurements collected during an intense grass fire experiment have revealed several crucial insights into the atmospheric disturbances associated with wildland fires. The passage of the fire front was marked by a dramatic surge in near-surface (5–6 m above ground) instantaneous temperature, recorded at 10 Hz frequency, surpassing 300 °C. This was coupled with vigorous updrafts exceeding 10 m s^{-1} and relatively less forceful downdrafts operating at half the speed. Ambient air was drawn towards the front as indicated by the shift of horizontal wind direction or an increase in lateral velocity component and gustiness, although overall horizontal wind speed show marginal changes. Behind the fire front, vertical motion subsided to ambient levels, yet the near-surface atmosphere remained more unstable than the ambient environment due to elevated temperatures. The fire-induced increase in temperature and horizontal convergence decreased with height, and much of the decrease occurred between the 5.8 m and 10 m levels.

Similar to temperature and vertical motion, the fire front passage was accompanied by a rapid increase in 10-second averaged upward vertical turbulent heat flux that reached nearly 400 kW m^{-2} and turbulent kinetic energy (TKE) that reached nearly 40 m^2 s^{-2}. Instantaneous heat flux exceeded 3 MW m^{-2}. A significant portion of the increase in TKE was attributed to the rise in vertical velocity variance, which displayed a distinct peak induced by the fire. While the horizontal velocity variance also experienced an upsurge during the fire, its magnitude may not surpass the local peaks observed outside the fire period.

A notable shift occurred in the vertical fluxes of horizontal momentum, transitioning from predominantly negative (downward) to some positive (upward) during fire front passage, suggesting higher momentum air in the combustion zone being transferred upward by turbulent eddies. The increase in the lateral component of vertical fluxes of horizontal momentum was much larger than that of the longitudinal component. While fire-induced TKE and particularly vertical heat fluxes decreased from the lowest tower level at 5.8 m to the next level at 10 m, the vertical fluxes of horizontal momentum and friction velocity increased slightly between the two levels. In addition, the peak values related to fire front passage were the absolute maxima for temperature, vertical velocity and variance, and vertical heat flux, yet they were local maxima for horizontal velocity and variance, TKE, vertical flux of horizontal momentum and friction velocity. These findings suggest that despite the substantial heat exchange of approximately 300–400 kW m^{-2} between the combustion zone and the atmosphere and the accompanying surge in vertical motion of about 10 m s^{-1}, the impact of the fire on horizontal velocities and the associated wind shear may not exhibit distinctive characteristics when compared to those observed in a daytime atmospheric boundary layer under windy conditions.

The fire front passage moved the turbulence regime from anisotropic towards isotropic. The vertical velocity distribution accompanying the fire front passage deviated significantly from Gaussian, with large positive skewness and kurtosis values indicating the presence of stronger, narrower updrafts surrounded by weaker, broader downdrafts. This asymmetry in updrafts and downdrafts associated with the fire front passage has important implications for scalar (smoke particles, heat and moisture) transport into and out of the combustion zone.

The tower placement downwind of the fire line was designed to capture the differential influence of heading and flanking fires. The data and analysis, however, failed to confirm the hypothesis that fire-induced perturbations due to a head fire would be more intense than those due to a flank fire. This underscores the challenge in isolating the effects of fire type on the ambient atmosphere in a real-world setting, where numerous factors, such as small-scale heterogeneity in fuel and atmospheric conditions, may come into play.

The results here provide, to our knowledge, the first in-situ observations of atmospheric turbulence during an intense grassfire under a Red Flag Warning, signifying the presence of weather conditions conducive to the rapid spread of wildfires, typically coinciding with burn bans and heightened fire danger across the affected regions. While the peak values in TKE, heat and momentum fluxes could be viewed as upper limits for prescribed fires, they may not fully encompass the extreme conditions of wildfires. Nevertheless, these findings hold valuable insights into fire-induced turbulence and could be useful for validating and improving turbulence parameterizations in fire-behavior and smoke-dispersion models.

CRediT authorship contribution statement

Shiyuan Zhong: Formal analysis, Investigation, Methodology, Writing – original draft, Writing – review & editing. **Melissa Gonzalez-Fuentes:** Data curation, Formal analysis, Investigation. **Craig B. Clements:** Writing – review & editing, Conceptualization, Data curation, Funding acquisition, Project administration, Supervision. **Xindi Bian:** Formal analysis, Investigation, Software, Visualization. **Warren E. Heilman:** Conceptualization, Funding acquisition, Writing – review & editing. **Joseph J. Charney:** Investigation. **Mario M. Valero:** Data curation, Visualization. **Adam K. Kochanski:** Conceptualization, Data curation. **Michael T. Kiefer:** Investigation.

Declaration of competing interest

The authors declare that they have no known competing financial interests or personal relationships that could have appeared to influence the work reported in this paper.

Data availability

Data will be made available on request.

Acknowledgements

This research was supported by the US Forest Service Northern Research Station (20-JV-11242306–070; 21-CS-11242306–055) and the US Department of Agriculture National Institute of Food and Agriculture Hatch project (1010691).

The authors extend their gratitude to the participants of the FireFluxII experiment for their invaluable contributions in collecting the data utilized in this study. The authors also wish to express their appreciation to the anonymous reviewers for their thoughtful and constructive feedback provided on the earlier version of the manuscript.

References

Abatzoglou, J.T., Williams, A.P., 2016. Impact of climate change on wildfires across western US forests. Proc. Nat. Acad. Sci. U.S.A. 113 (42), 11770–11775. https://doi.org/10.1073/pnas.1607171113.

Ahmad, A.D., Akafuah, N.K., Forthofer, J., Fuchihata, M., Hirasawa, T., Kuwana, K., Nakamura, Y., Sekimoto, K., Saito, K., Williams, F.A., 2023. Large-scale fire whirl and forest fire disasters: awareness, implications, and the need for developing preventative methods. Front. Mech. Eng. 9, 1045542 https://doi.org/10.3389/fmech.2023.1045542.

Balch, J.K., Bradley, B.A., Abatzoglou, J.T., Nagy, R.C., Fusco, E.J., Mahood, A.L., 2017. Human-started wildfires expand the fire niche across the United States. Proc. Nat. Acad. Sci. U.S.A. 114 (11), 2946–2951. https://doi.org/10.1073/pnas.1617394114.

Clark, K.L., Heilman, W.E., Skowronski, N.S., Gallagher, M., Mueller, E., Hadden, R.M., Simeoni, A., 2020. Fire Behavior, fuel consumption, and turbulence and energy exchange during prescribed fires in pitch pine forests. Atmosphere (Basel) 11, 242. https://doi.org/10.3390/atmos11.

Clark, T.L., Jenkins, M.A., Coen, J., Packham, D., 1996. A coupled atmosphere-fire model: convective feedback on fire-line dynamics. J. Appl. Meteorol. 35, 875–901. https://doi.org/10.1175/1520-0450(1996)035<0875:ACAMCF>2.0.CO;2.

Clements, C.B., Seto, D., 2015. Observations of fire-atmosphere interactions and near-surface heat transport on a slope. Bound.-Layer Meteorol 154, 409–426.

Clements, C.B., Zhong, S., Goodrick, S., Li, J., Potter, B.E., Bian, X., Heilman, W.E., Charney, J.J., Perna, R., Jang, M., Lee, D., Patel, M., Street, S., Aumann, G., 2007. Observing the dynamics of wildland grass fires: fireFlux— A field validation experiment. Bull. Amer. Meteorol. Soc. 88 (9), 1369–1382. https://doi.org/10.1175/BAMS-88-9-1369.

Clements, C.B., Zhong, S., Bian, X., Heilman, W.E., Byun, D.W., 2008. First observations of turbulence generated by grass fires. J. Geophys. Res. 113, D22102. https://doi.org/10.1029/2008JD010014.

Clements, C.B., Kochanski, A.K., Seto, D., Davis, B., Camacho, C., Lareau, N.P., Contezac, J., Restaino, J., Heilman, W.E., Krueger, S.K., Butler, B., Ottmar, R.D., Vihnanek, R., Flynn, J., Filippi, J.B., Barboni, T., Hall, D.E., Mandel, J., Jenkins, M. A., O'Brien, J., Hornsby, B., Teske, C., 2019. The FireFlux II experiment: a model-guided field experiment to improve understanding of fire–atmosphere interactions and fire spread. Int. J. Wildland Fire 28, 308–326. https://doi.org/10.1071/WF18089.

Coen, J.L., Cameron, M., Michalakes, J., Patton, E.G., Riggan, J.P., Yedinak, K.M., 2013. WRF-Fire: coupled weather–wildland fire modeling with the Weather Research and Forecasting model. J. Appl. Meteor. Climatol. 52, 16–38. https://doi.org/10.1175/JAMC-D-12-023.1.

Desai, A., Goodrick, S., Banerjee, T., 2022. Investigating the turbulent dynamics of small-scale surface fires. Sci. Rep. 12 (1), 10503. https://doi.org/10.1038/s41598-022-13226-w.

Dupuy, J.L., 1995. Slope and fuel load effects on fire behavior: laboratory experiments in pine needles fuel beds. Int. J. Wildland Fire. 5, 153–165. https://doi.org/10.1071/WF9950153.

Filippi, J.B., Pialat, X., Clements, C.B., 2013. Assessment of ForeFire/Meso-NH for wildland fire/atmosphere coupled simulation of the FireFlux experiment. Proc. Combust. Inst. 34 (2), 2633–2640. https://doi.org/10.1016/j.proci.2012.07.022.

Filippi, J.B., Bosseur, F., Mari, C., Lac, C., 2018. Simulation of a large wildfire in a coupled fire-atmosphere model. Atmosphere (Basel) 9 (6), 218.

Finney, M.A., Cohen, J.D., McAllister, S.S., Jolly, W.M., 2011. On the simulating of grassfires. Int. J. Wildland Fire 20 (6), 784–800.

Finney, M., Pearce, G., Strand, T., Katurji, M., Clements, C., 2018. New Zealand prescribed fire experiments to test convective heat transfer in wildland fires. In: Advances in Forest Fire Research 2018. Proceedings of the VII International Conference on Forest Fire Research, pp. 10–16.

Forthofer, J.M., Goodrick, S.L., 2011. Review of vortices in wildland fire. J. Combustion 1–14. https://doi.org/10.1155/2011/984363.

Forthofer, J.M., 2019. Fire tornadoes. Scientific Amer 321, 60–67.

Fromm, M., Lindsey, D.T., Servranckx, R., Yue, G., Trickl, T., Sica, R., Doucet, P., Godee, B., 2010. The untold story of pyrocumulonimbus. Bull. Amer. Meteorol. Soc. 91 (9), 1193–1210. https://doi.org/10.1175/2010BAMS3004.1.

Halofsky, J.E., Peterson, D.L., Harvey, B.J., 2020. Changing wildfire, changing forests: the effects of climate change on fire regimes and vegetation in the Pacific Northwest. USA. Fire Ecol 16, 4. https://doi.org/10.1186/s42408-019-0062-8.

Heilman, W.E., Clements, C.B., Seto, D., Bian, X., Clark, K.L., Skowronski, N.S., Hom, J. L., 2015. Observations of fire induced turbulence regimes during low-intensity wildland fires in forested environments: implications for smoke dispersion. Atmos. Sci. Lett. 16, 453–460. https://doi.org/10.1002/asl.581.

Heilman, W.E., Bian, X., Clark, K.L., Skowronski, N.S., Hom, J.L., Gallagher, M.R., 2017. Atmospheric turbulence observations in the vicinity of surface fires in forested environments. J. Appl. Meteorol. Climatol. 56, 3133–3150.

Heilman, W.E., Bian, X., Clark, K.L., Zhong, S., 2019. Observations of turbulent heat and momentum fluxes during wildland fires in forested environments. J. Appl. Meteorol. Climatol. 58, 813–829. https://doi.org/10.1175/JAMC-D-18-0199.1.

Heilman, W.E., Banerjee, T., Clements, C.B., Clark, K.L., Skowronski, N.S., Zhong, S., Bian, X., 2021a. Observations of sweep-ejection dynamics for heat and momentum fluxes during wildland fires in forested and grassland environments. J. Appl. Meteorol. Climatol. 60, 185–198. https://doi.org/10.1175/JAMC-D-20-0086.1.

Heilman, W.E., 2021b. Atmospheric turbulence in wildland fire environments: implication for fire behavior and smoke dispersion. Fire Mang. Today 79 (1), 24–29.

Hiers, J.K., O'Brien, J.J., Varner, J.M., Butler, B.W., Dickinson, M., Furman, J., Gallagher, M., Godwin, D., Goodrick, S.L., Hood, S.M., Hudak, A., Kobziar, L.N., Linn, R.R., Loudermilk, E.L., McCaffery, S., Robertson, K., Rowell, E.M., Skowronski, N., Watts, A.C., Yedinak, K.M., 2020. Prescribed fire science: the case for a refined research agenda. Fire Ecol 16, 11. https://doi.org/10.1186/s42408-020-0070-8.

Jonko, A.K., Yedinak, K.M., Conley, J.L., Linn, R.R., 2021. Sensitivity of grass fires burning in marginal conditions to atmospheric turbulence. J. Geophys. Res.: Atmos 126, e2020JD033384.

Katurji, M., Noonan, B., Zhang, J., Valencia, A., Shumacher, B., Kerr, J., Strand, T., Pearce, G., Zawar-Reza, P., 2022a. Atmospheric turbulent structures and fire sweeps during shrub fires and implications for flaming zone behavior. Int. J. Wildland Fire 32 (1), 43–55. https://doi.org/10.1071/WF22100.

Katurji, M., Zhang, J., Satinsky, A., McNair, H., Schumacher, B., Strand, T., Valencia, A., Finney, M., Pearce, G., Kerr, J., Seto, D., Wallace, H., Zawar-Reza, P., Dunker, C., Clifford, V., Melnik, K., Grumstrup, T., Forthofer, J., Clements, C., 2022b. Turbulent thermal image velocimetry at the immediate fire and atmospheric interface. J. Geophy. Res. 126 (24), e2021JD035393 https://doi.org/10.1029/2021JD035393.

Kiefer, M.T., Charney, J.J., Zhong, S., Heilman, W.E., Bian, B., Mathewson, T.O., 2020. A multiscale numerical modeling study of smoke dispersion and the ventilation index in Southwestern Colorado. Atmosphere (Basel) 11, 846. https://doi.org/10.3390/atmos11080846.

Kochanski, A.K., Jenkins, M.A., Mandel, J., Beezley, J.D., Clements, C.B., Krueger, S., 2013. Evaluation of WRF-SFIRE performance with field observations from the FireFlux experiment. Geosci. Model Dev. 6, 1109–1126. https://doi.org/10.5194/gmd-6-1109-2013.

Kuwana, K., Sekimoto, K., Saito, K., Williams, F.A., 2008. Scaling fire whirls. Fire Safety J 43, 252–257. https://doi.org/10.1016/j.firesaf.2007.10.006.

Lareau, N.P., Nauslar, N.J., Bentley, E., Roberts, M., Emmerson, S., Brong, B., Mehle, M., Wallman, J., 2022. Fire-generated tornadic vortices. Bull. Amer. Meteor. Soc. E1296–E1320. https://doi.org/10.1175/BAMS-D-21-0199.1.

Linn, R.R., Goodrick, S.L., Brambilla, S., Brown, M.J., Middleton, R.S., O'Brien, J.J., Hiers, J.K., 2020. QUIC-fire: a fast-running simulation tool for prescribed fire

planning. Environ. Model. Software. 125, 104616 https://doi.org/10.1016/j.envsoft.2019.104616.
Liu, Y., Smith, J.R., Anderson, S.M., Thompson, L.C., Martinez, A.B., 2017. Climate change and wildfire: a review of fire effects and management implications. Forests 8 (3), 63.
Morandini, F., Silvani, X., Rossi, L., Santoni, P., Simeoni, A., Balbi, J., Rossi, J.L., Marcelli, T., 2006. Fire spread experiment across Mediterranean shrub: influence of wind on flame front properties. Fire Safety J 41, 229–235. https://doi.org/10.1016/j.firesaf.2006.01.006.
Ottmar, R.D., Hiers, J.K., Butler, B.W., Clements, C.B., Dickinson, M.B., Hudak, A.T., O'Brien, J.J., Potter, B.E., Rowell, E.M., Strand, T.M., Zajkowski, T.J., 2016. Measurements, datasets, and preliminary results from the RxCADRE project –2008, 2011, and 2012. Int. J. Wildland Fire 25, 1–9. https://doi.org/10.1071/WF14161.
Peterson, D.A., Campbell, J.R., Hyer, E.J., Fromm, M.D., Kablick, G.P., Cossuth, J.H., DeLand, M.T., 2018. Wildfire-driven thunderstorms cause a volcano-like stratospheric injection of smoke. npj Climate Atmos. Sci. 1, 30. https://doi.org/10.1038/s41612-018-0039-3.
Peterson, D., Fromm, M., McRae, R., Campbell, J., Hyer, E., Taha, G., Camacho, C., Kablick, G., Schmidt, C., DeLand, M., 2021. Australia's black summer pyrocumulonimbus super outbreak reveals potential for increasingly extreme stratospheric smoke events. npj Climate Atmos. Sci. 4, 38. https://doi.org/10.1038/s41612-021-00192-9.
Potter, B.E., 2002. A dynamics based view of atmosphere - fire interactions. Int. J. Wildland Fire 11 (4), 247. https://doi.org/10.1071/WF02008.
Potter, B.E., 2012. Atmospheric interactions with wildland fire behavior. Basic surface interactions, vertical profiles and synoptic structures. Int. J. Wildland Fire 21, 779–801. https://doi.org/10.1071/WF11128.
Rodriguez, B., Lareau, N.P., Kingsmill, D.E., Clements, C.B., 2020. Extreme pyroconvective updrafts during a megafire. Geophys. Res. Lett. 47, e2020GL089001 https://doi.org/10.1029/2020GL089001.
Seto, D., Clements, C.B., 2011. Fire whirl evolution observed during a valley wind-sea breeze reversal. J. Combustion 2011, 1–12. https://doi.org/10.1155/2011/569475.
Seto, D., Clements, C.B., Heilman, W.E., 2013. Turbulence spectra measured during fire front passage. Ag. Forest Meteorol. 169, 195–210. https://doi.org/10.1016/j.agrformet.2012.09.015.
Seto, D., Strand, T., Clements, C.B., Thistle, H., Mickler, R.A., 2014. Wind and plume thermodynamic structure during low-intensity subcanopy fires. Agri. Forest Meteorol. 198-199, 53–61. https://doi.org/10.1016/j.agrformet.2014.07.006.
Stull, R.B., 1988. An Introduction to Boundary Layer Meteorology. Kluwer Acad. Pub., New York, p. 666.
Sullivan, A.L., 2009. Wildland surface fire spreading modeling, 1990-2007. 1. Physical and quasi-physical models. Int. J. Wildland Fire 349–368.
Sun, R., Krueger, S.K., Jenkins, M.A., Zulauf, M.A., Charney, J.J., 2009. The importance of fire-atmosphere coupling and boundary layer turbulence to wildfire spread. Int. J. Wildland Fire 18 (1), 50–56. https://doi.org/10.1071/WF07072.
Wilczak, J.M., Oncley, S.P., Stage, S.A., 2001. Sonic anemometer tilt correction algorithms. Bound.-Layer Meteorol 99, 127–150. https://doi.org/10.1023/A:1018966204465.
Wilson, J.D., Flesch, T.K., 1997. Trajectory curvature as a selction criterion for valid Lagrangian stochastic dispersion models. Bound.-Layer Meterol 84, 411–425. https://doi.org/10.1023/A:1000474206967.
Zhang, J., Katurji, M., Zawar-Reza, P., Strand, T., 2023. The role of helicity and fire–atmosphere turbulent energy transport in potential wildfire behavior. Int. J. Wildland Fire 32 (1), 29–42. https://doi.org/10.1071/WF22101.
Zhong, S., Wang, T., Sciusco, P., Shen, M., Pei, L., Nikolic, J., McKeehan, K., Kashongwe, H., Hatami-Bahman-Beiglou, P., Camacho, K., Akanga, D., Charney, J., Bian, B., 2021. Will land use land cover change drive atmospheric conditions to become more conducive to wildfires in the United States? Int. J. Climatol. 41, 3578–3597. https://doi.org/10.1002/joc.7036.